High-speed quantum cascade detector characterized with a mid-infrared femtosecond oscillator

JOHANNES HILLBRAND,[1,3] (iD) LÉONARD MATTHIEU KRÜGER,[2]
SANDRO DAL CIN,[1] HEDWIG KNÖTIG,[1] (iD) JONAS HEIDRICH,[2] (iD)
AARON MAXWELL ANDREWS,[1] (iD) GOTTFRIED STRASSER,[1] (iD)
URSULA KELLER,[2] (iD) AND BENEDIKT SCHWARZ[1,4] (iD)

[1]*Institute of Solid State Electronics, TU Wien, Gusshausstrasse 25-25a, 1040 Vienna, Austria*
[2]*Institute for Quantum Electronics, ETH Zürich, CH-8093 Zürich, Switzerland*
[3]*johannes.hillbrand@tuwien.ac.at*
[4]*benedikt.schwarz@tuwien.ac.at*

Abstract: Quantum cascade detectors (QCD) are photovoltaic mid-infrared detectors based on intersubband transitions. Owing to the sub-picosecond carrier transport between subbands and the absence of a bias voltage, QCDs are ideally suited for high-speed and room temperature operation. Here, we demonstrate the design, fabrication, and characterization of 4.3 μm wavelength QCDs optimized for large electrical bandwidth. The detector signal is extracted via a tapered coplanar waveguide (CPW), which was impedance-matched to 50 Ω. Using femtosecond pulses generated by a mid-infrared optical parametric oscillator (OPO), we show that the impulse response of the fully packaged QCDs has a full-width at half-maximum of only 13.4 ps corresponding to a 3-dB bandwidth of more than 20 GHz. Considerable detection capability beyond the 3-dB bandwidth is reported up to at least 50 GHz, which allows us to measure more than 600 harmonics of the OPO repetition frequency reaching 38 dB signal-to-noise ratio without the need of electronic amplification.

1. Introduction

There is a growing interest in sensitive and high-speed photodetectors operating in the mid-infrared (MIR) range. Demanding applications are found in different fields including spectroscopy [1,2], free-space optical telecommunication [3] and frequency comb research [4–6]. In dual-comb spectroscopy, fast MIR detectors are required to detect the multi-heterodyne beating between the comb lines. The temporal resolution of this technique is particularly high and ultimately only limited by the bandwidth of the photodetector - provided that frequency combs with large repetition rate are available [7]. MIR detectors with 20 GHz or more electrical bandwidth will enable spectroscopic real-time monitoring of chemical reactions [8,9] on time-scales as short as tens of nanoseconds. Furthermore, fast photodetectors have become an invaluable tool to measure the phase-coherence and timing jitter [10–13] of frequency combs and to reconstruct the waveform of mode-locked lasers [14,15].

Intersubband photodetectors are based on transitions between electronic states in the conduction band and are ideally suited for high-speed operation in the long-wavelength range. Band structure engineering allows to tailor the spectral response from 1.55 μm [16] over MIR wavelengths [17] to the Terahertz (THz) range [18]. Transport between the subbands typically occurs on the picosecond timescale dominantly due to efficient scattering with longitudinal-optical (LO) phonons [19] and resonant tunneling. This property enables electrical detection bandwidths up

to several tens of Gigahertz (GHz). Quantum well infrared photodetectors (QWIPs) [20] are among the most prominent and well-studied types of intersubband detectors. The active region of a QWIP consists of a biased superlattice acting as a photoconductor. It was shown that the electrical detection bandwidth is determined by the lifetime of the upper state in the quantum wells, which is on the order of a few picoseconds [21]. As a result, heterodyne detection up to 110 GHz was demonstrated using a QWIP connected to a coplanar microwave transmission line [22]. At elevated temperatures, however, the detectivity of QWIPs decreases exponentially due to thermally activated dark current. Recent work has shown that this issue can be mitigated by embedding the QWIP into a patch array antenna [23,24]. This technique effectively reduces the electrical area and the dark current of the detector and thus allows room temperature operation.

Quantum cascade detectors (QCDs) [17] are similar to photovoltaic QWIPs [25]. Instead of an external bias, QCDs make use of a series of subbands spaced by the LO phonon energy (Fig. 1(a) [26]). This LO phonon ladder can be seen as a built-in field to extract the photoexcited electrons from the upper state of the optical transition and inject them into the ground state of the next period [27]. As a consequence, the dominant noise mechanism of QCDs is thermal Johnson noise related to the detector resistance, which is favorable for room temperature operation. Similarly to QWIPs, carrier transport in QCDs occurs on the picosecond timescale, which enables high-speed heterodyne detection at room temperature [28,29]. It should be noted that interband cascade infrared photodetectors (ICIPs) based on type-II broken band gap structures are also emerging as promising candidate for high-speed and spectrally broadband detectors [30–33] and 7 GHz bandwidth has been reported recently [34].
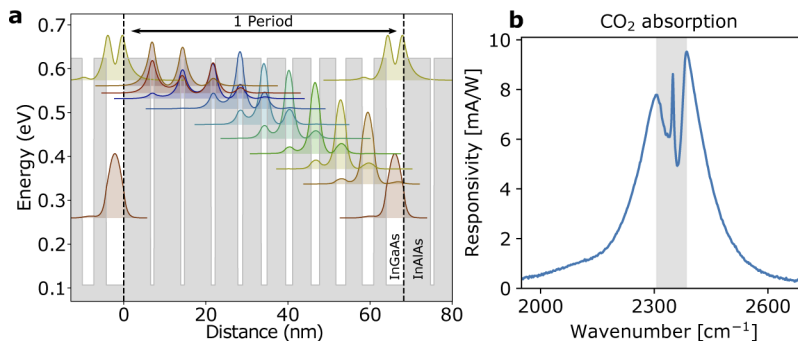

Fig. 1. a: simulated band structure of the QCD based on InGaAs/InAlAs lattice-matched to InP. Excited electrons are extracted from the active quantum well and injected into the next period via a LO phonon ladder. The first three states of the extraction region are separated by less than the LO phonon energy to enhance the extraction probability. Further, the energy separation between lowest state of the LO phonon ladder and the ground state of the optical transition is larger than the LO phonon energy to prevent thermal backfilling of carriers into the injector region. The design of this structure can be found in Ref. [26]. **b**: responsivity of a 100 μm x 100 μm large QCD mesa at room temperature (295 K). The data was obtained by recording the QCD spectrum with a Fourier transform infrared (FTIR) spectrometer and a globar. The power incident on the QCD was normalized by mapping the focal spot of the globar with a motorized translation stage and recording the globar spectral density with a calibrated thermal powermeter. The shaded area corresponds to the CO_2 absorption band.

In this work, we demonstrate high-speed QCDs operating up to at least 50 GHz with a 3-dB bandwidth above 20 GHz. The peak responsivity of the fabricated detectors near 4.3 μm wavelength reaches almost 10 mA/W at room temperature (Fig. 1(b)). The QCDs are connected to an on-chip tapered coplanar waveguide (CPW) matched to 50 Ω impedance, which allows

packaging with a microwave end-launch connector. We present the first temporal characterization of QCDs with a femtosecond MIR oscillator, revealing a fast impulse response of only 13.4 ps.

2. Quantum cascade detectors optimized for radio frequency operation

In order to exploit the high-speed detection capabilities of QCDs, the parasitic components of the circuit connected to the detector have to be minimized. An equivalent circuit of the QCD and its parasitic circuit is shown in Fig. 2(a). The electrical power frequency response $R(\omega)$ of this system is given by

$$R(\omega) = \left| \frac{U_{\text{out}}(\omega)}{U_{\text{out}}(\omega = 0)} \right|^2 = \frac{1}{\left(1 + \frac{Z_L}{R_D} - \omega^2 L C_D \right)^2 + \omega^2 \left(\frac{L}{R_D} + Z_L C_D \right)^2} \tag{1}$$
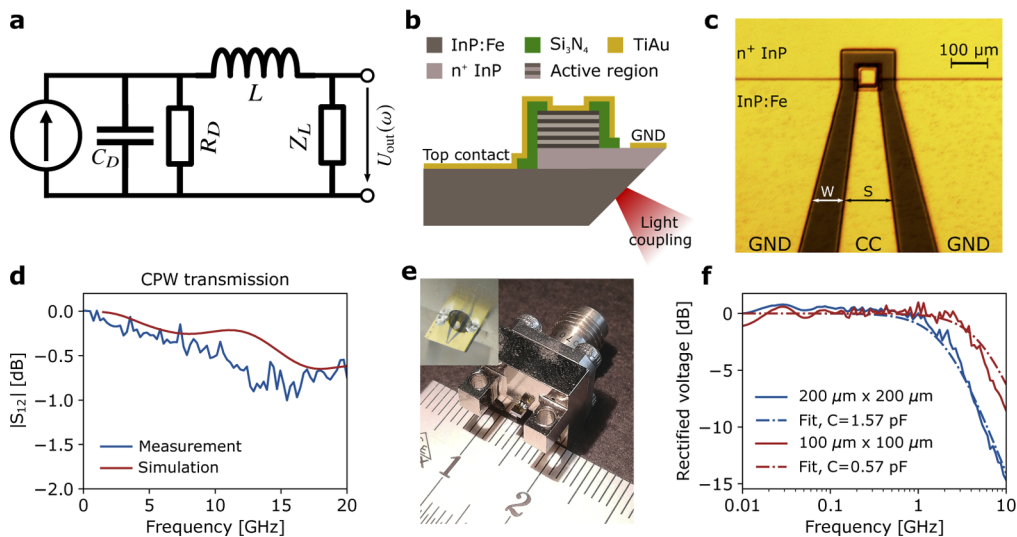

Fig. 2. High-speed QCD connected to a tapered coplanar waveguide. a: equivalent circuit of the QCD. R_D and C_D: parasitic resistance and capacitance of the detector. L: parasitic inductance caused by wire bonds. Z_L: load resistance (50 Ω). **b**: lateral schematic of the fabricated QCDs. The detector mesas are etched using a H_3PO_4:H_2O_2:H_2O mixture (3:2:40 mass fractions). Subsequently, the highly-doped contact layer (n^+ InP) is removed on one side of the mesa and a 1.5 μm thick Si_3N_4 layer is used to passivate the sidewalls of the detector. Finally, the CPW consisting of a top contact (or center conductor, CC) and two ground planes (GND) is sputtered onto the chip. **c**: microscope image of the detector mesa connected to a tapered CPW. **d**: Measured (blue line) and simulated (red line) transmission through a 2 mm long CPW tapered from 250 μm to 25 μm CC width. **e**: photograph of a fully packaged high-speed QCD soldered to a 2.92 mm end-launch connector. The inset shows a microscope image of the soldered QCD chip. **f**: rectified voltage for 200 μm x 200 μm (blue line) and 100 μm x 100 μm (red line) large QCD mesas. Both curves show a lowpass behaviour due to the parasitic capacitance of the active region. The dashed lines correspond to a fit using Eq. (1).

R_D and C_D are the parasitic resistance and capacitance of the detector, respectively, and L is the parasitic inductance. Z_L is the load resistance ($Z_L = 50$ Ω). This circuit shows a low-pass behaviour, whose 3-dB bandwidth depends strongly on the parasitic inductance and capacitance. The latter can be minimized by decreasing the detector area. Parasitic inductance is mainly caused by wire bonds connected to the detector. The LC resonance introduced by wire bonds and

the detector capacitance is particularly detrimental for the high-frequency performance, because it causes a $1/\omega^4$ (40 dB/decade) decrease of the frequency response above the cut-off frequency.

In order to avoid wire bonds, we fabricated QCDs connected to a coplanar waveguide (CPW, Figs. 2(b) and 2(c)). The center conductor (CC) of the CPW is connected to the top contact of the detector and surrounded by two ground planes (GND). Due to a 1.5 μm thick Si_3N_4 passivation layer around the sidewalls of the detector, the CPW does not require an air bridge connector to the mesa as reported in other works [35]. The impedance of the CPW must be matched to 50 Ω to avoid RF reflections. This is achieved by adapting the gap width W to the CC width S (Fig. 2(c)). The latter is then tapered from the dimensions of the detector mesa (25 μm) to the diameter of the pin of a commercial microwave connector (250 μm) while maintaining 50 Ω impedance. Using COMSOL Multiphysics simulations, we find an approximately linear taper curve $W(S)$ for a 320 μm thick InP substrate.

$$W(S)|_{Z=50\,\Omega} \approx 6.5\,\mu m + 0.53 \cdot S\,[\mu m] \qquad \text{for} \qquad 25\,\mu m \leq S \leq 250\,\mu m \qquad (2)$$

Gold is not deposited on the backside of the chip, as this would result in a microstrip-like mode of the CPW, which does not allow tapering of the CC while maintaining 50 Ω impedance. Furthermore, the two ground planes should be connected behind the detector mesa to avoid exciting the odd waveguide mode of the CPW, which shows large dispersion at frequencies higher than 10 GHz. For similar reasons, the length of the CPW should be kept as small as possible, because the ground planes cannot be connected by conducting vias like it is usually done in printed circuit boards. Figure 2(d) shows the transmission through a 2 mm long tapered CPW measured using an RF synthesizer, a microwave spectrum analyzer (MSA) and two RF probes to inject and extract the signal. The loss stays below 1 dB up to 20 GHz and is in good agreement with the simulated $|S_{12}|$ parameter.

The CPW is finally connected to a commercial 2.92 mm end-launch connector using a low-temperature SnBi solder paste as shown in Fig. 2(e). Hence, the high-speed QCDs are fully packaged in a volume of roughly 1 cm^3 and can be connected to a microwave network for characterization and RF signal processing without the need for RF probes.

We measured the capacitance of two 200 μm x 200 μm and 100 μm x 100 μm large QCD mesas using microwave rectification [21] (Fig. 2(f)). In both cases, the rectified voltage shows a lowpass response caused by the parasitic capacitance of the QCD. The resistance of the QCDs varies between 200 Ω and 15 kΩ for mesa sizes between 200 μm and 25 μm, which can be neglected compared to the 50 Ω impedance of the transmission line. We estimate that the RC cut-off frequency of the smallest mesa (25 μm x 25 μm) is above 60 GHz (corresponding to C<0.05 pF), which is beyond the bandwidth of our rectification setup. Thus, we resort to optical methods for measuring the frequency response of the smallest QCD.

3. Impulse and frequency response

There are multiple methods to characterize the frequency response of fast photodetectors optically. A regularly employed technique uses the heterodyne signal between two tunable single-mode lasers [28]. When both lasers are combined on the photodetector, they generate a beating at their difference frequency. The frequency response of the detector is obtained by tuning the frequency of one laser and recording the beatnote amplitude as function of its frequency.

Another method, which allows to retrieve even more information, uses short optical pulses and a fast oscilloscope to record the impulse response of the photodetector, as shown in Fig. 3(a). This technique was widely used to investigate the frequency response of QWIPs [36,37]. The equivalent circuit of the QCD in Fig. 2(a) is a stable linear time-invariant system. Thus, its frequency response is given by the Fourier transform of the impulse response.

We measured the latter by coupling mid-infrared femtosecond pulses into the QCD via a 45 ° polished facet with an aspheric lens. The detector signal is recorded using a 50 GHz sampling
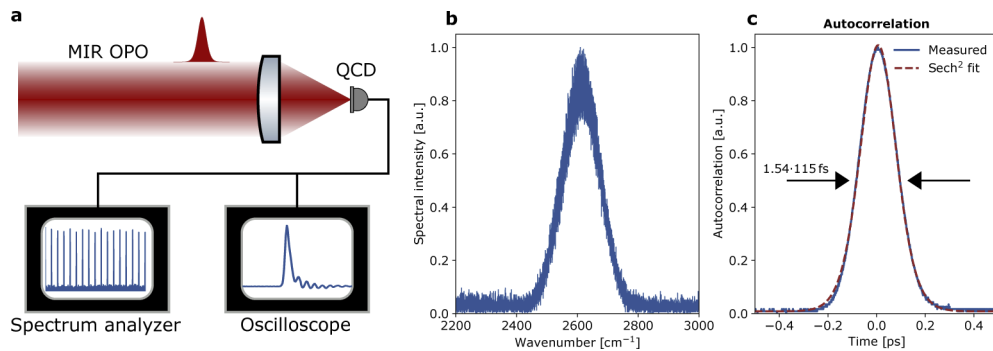
Fig. 3. **a**: experimental setup for measuring the impulse response of the QCD using femtosecond pulses. **b**: optical spectrum of the OPO operating around $2600\,cm^{-1}$ (3.85 μm). The FWHM of the spectrum is approximately $130\,cm^{-1}$, suggesting a transform limited pulse duration of 115 fs. **c**: autocorrelation of the OPO pulses operating at 3.3 μm. Assuming a sech^2 shape, a pulse width of 115 fs is found. At 3.85 μm, the response of the InGaAs detector used in the autocorrelator is decreased considerably. In addition the available optical power from the OPO decreases significantly leading to very low signal-to-noise ratio. Under these conditions, we estimate that the pulse width is increased to 140 fs.

oscilloscope and a 50 GHz microwave spectrum analyzer (MSA). The optical pulses are generated by a femtosecond pulsed optical parametric oscillator (OPO, Radiantis Oria XT) with a pulse repetion rate of 80.2 MHz. The non-resonant idler was tuned close to its maximum wavelength at 3.85 μm ($2600\,cm^{-1}$, Fig. 3(b)), where the incident average power is roughly 3 mW. The soliton shaped optical spectrum was centered at 3.85 μm with a full-width at half maximum of $130\,cm^{-1}$ (Fig. 3(b)). The measured pulse duration ranges between 115-140 fs depending on the idler wavelength (Fig. 3(c)). This can be regarded as a good approximation for δ-pulses, because the microwave frequency bandwidth of the pulses is given by the inverse of their pulse duration, which is more than an order of magnitude larger than the bandwidth of the oscilloscope.

Figure 4(a) displays the impulse response of a 25 μm x 25 μm QCD mesa. The oscilloscope trace consists of a 13.4 ps short initial burst followed by a negative voltage dip. This phenomenon was also observed in photovoltaic QWIPs [38], where it was attributed to thermionic emission of carriers in the extractor region back to the excited state of the optical transition. This gives rise to transport in the opposite direction of the photocurrent. However, we observe that the magnitude of this ringing depends strongly on how the QCD is mounted on the end-launch connector and its connection to the RF cable. An air gap between the QCD chip and the dielectric of the end-launch connector as well as overtightening the RF cables should be avoided to minimize pulse ringing. The impulse response recorded over 15 ns (Fig. 4(b)) shows two subsequent pulses spaced by the cavity roundtrip period of the OPO. The signal around 5 ns is caused by reflections in the cable.

The frequency response of the QCD is given by the absolute square of the Fourier transform of its impulse response and shows a 3-dB cut-off frequency at 21 GHz (Fig. 4(c)). This result includes the losses of the RF cables and the bias-T used to connect the QCD to the oscilloscope. The parasitic capacitance is found to be roughly 0.18 pF by fitting Eq. (1) to the measured frequency response. This is considerably larger than expected by extrapolating the rectification curves in Fig. 2(f) to a 25 μm x 25 μm mesa size. This observation potentially indicates that the electrical bandwidth is not limited by the parasitic capacitance of the QCD anymore, but rather by the intrinsic response time of its active region. Nevertheless, significant detection capability extends up to at least 50 GHz (limited by the oscilloscope), because no wire bonds were used.

The fundamental pulse repetion rate of the OPO at 80.2 MHz and its 620 higher harmonics can be extracted from the QCD photocurrent using a microwave spectrum analyzer as shown
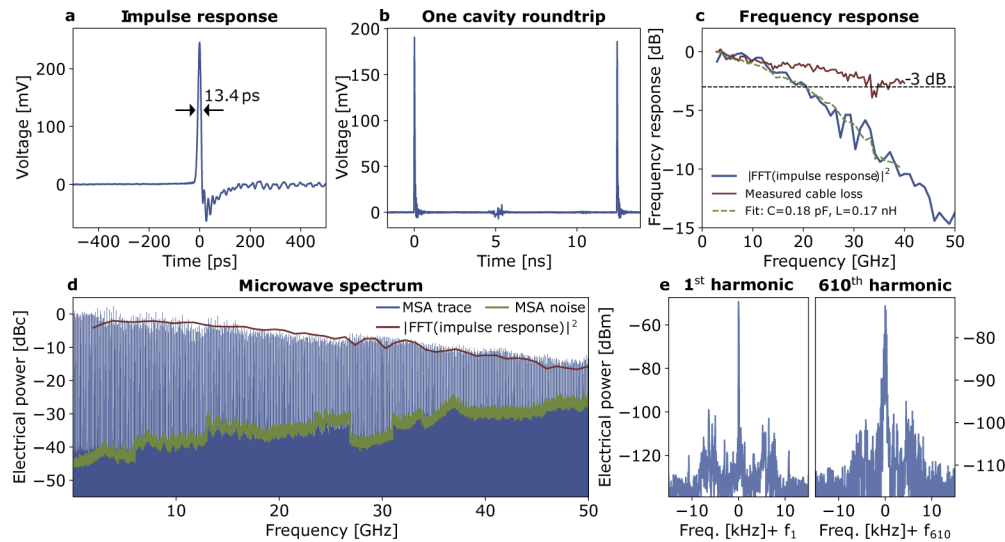
Fig. 4. Frequency response of high-speed QCDs. a: impulse response of a 25 μm square mesa showing a FWHM of 13.4 ps. **b**: impulse response recorded over a cavity roundtrip period of the OPO. Two subsequent pulses are visible. **c**: frequency response of the QCD (blue line), and losses of the coaxial cable and bias-T connecting the QCD to the oscilloscope (red line). The green dashed line constitutes a fit using Eq. (1) and the measured cable loss. The frequency response is only plotted for f>2 GHz, because the impulse response in **a** resembles a high-pass behaviour due to the negative voltage dip. **d**: Harmonics of the OPO beatnote up to 50 GHz (blue line) compared to the frequency response from **c** (red line). At low frequencies, the amplitude envelope shows periodic modulations with a period of roughly $3 \cdot f_{rep}$ (240 MHz). This is attributed to reflections at the connector of the MSA, which leads to standing waves in the 50 cm long coaxial cable connected to the QCD (Huber+Suhner Multiflex 141, roundtrip frequency≈210 MHz). The amplitude envelope becomes flatter at higher frequencies due to the growing RF losses of the cable, which prevent standing waves from forming. The decreasing SNR at higher frequencies is mainly due to the increased noise-floor of the MSA (green line). The resolution bandwidth was 30 kHz. **e**: first and 610th harmonic of the OPO detected with 80 dB and 38 dB signal-to-noise ratio, respectively. f_1=80.2 MHz. The resolution bandwidth was 30 Hz.

in Fig. 4(d). As expected, the envelope of the radio frequency spectrum is in good agreement with the Fourier transform of the impulse response. The agreement between the curves could be further improved by eliminating standing waves in the coaxial cable [39]. Figure 4(e) shows a detailed zoom on the first and 610th harmonic of the OPO beatnote. Despite the increased noise of the MSA at higher frequencies, these beat tones can be measured with a signal-to-noise ratio (SNR) of 80 dB and 38 dB, respectively. This result is particularly astonishing keeping in mind that the average power of the OPO is only 3 mW and the pulse spectrum is not exactly matched to the peak of the detector spectrum. The SNR could be further increased with a high bandwidth electronic amplifier. Moreover, it can be seen that the width of the 610th harmonic is increased, which can be attributed to phase-noise. This could be used in future work to sensitively characterize the phase-noise of MIR frequency combs using the von der Linde method [11].

4. Conclusion and outlook

We have demonstrated the capabilities of quantum cascade detectors as high-speed MIR photodetectors. They operate at room temperature and without bias voltage. A tapered microwave

transmission line allows convenient packaging in a small volume using a standard 2.92 mm connector. Design rules for the CPW have been presented. The fabricated QCDs operate up to 50 GHz with a 3-dB bandwidth around 21 GHz. By fabricating even smaller mesas in future work, it could be investigated whether the observed detection bandwidth is still limited by the parasitic capacitance or by the intrinsic response of the QCD active region. Furthermore, the pulse ringing visible in the impulse response will be improved by refining the soldering procedure of the detector chip to the end-launch connector. In conclusion, QCDs constitute a promising tool for characterizing mode-locked semiconductor lasers [40–43] in the mid-infrared region with repetition frequencies exceeding 10 GHz.

Disclosures. The authors declare no conflicts of interest.

References

1. I. Coddington, N. Newbury, and W. Swann, "Dual-comb spectroscopy," Optica **3**(4), 414 (2016).
2. G. Villares, A. Hugi, S. Blaser, and J. Faist, "Dual-comb spectroscopy based on quantum-cascade-laser frequency combs," Nat. Commun. **5**(1), 5192 (2014).
3. S. Blaser, D. Hofstetter, M. Beck, and J. Faist, "Free-space optical data link using peltier-cooled quantum cascade laser," Electron. Lett. **37**(12), 778 (2001).
4. T. Udem, R. Holzwarth, and T. W. Hänsch, "Optical frequency metrology," Nature **416**(6877), 233–237 (2002).
5. H. Telle, G. Steinmeyer, A. Dunlop, J. Stenger, D. Sutter, and U. Keller, "Carrier-envelope offset phase control: A novel concept for absolute optical frequency measurement and ultrashort pulse generation," Appl. Phys. B **69**(4), 327–332 (1999).
6. D. J. Jones, "Carrier-envelope phase control of femtosecond mode-locked lasers and direct optical frequency synthesis," Science **288**(5466), 635–639 (2000).
7. D. Kazakov, M. Piccardo, Y. Wang, P. Chevalier, T. S. Mansuripur, F. Xie, C. en Zah, K. Lascola, A. Belyanin, and F. Capasso, "Self-starting harmonic frequency comb generation in a quantum cascade laser," Nat. Photonics **11**(12), 789–792 (2017).
8. J. L. Klocke, M. Mangold, P. Allmendinger, A. Hugi, M. Geiser, P. Jouy, J. Faist, and T. Kottke, "Single-shot sub-microsecond mid-infrared spectroscopy on protein reactions with quantum cascade laser frequency combs," Anal. Chem. **90**(17), 10494–10500 (2018).
9. N. H. Pinkowski, Y. Ding, C. L. Strand, R. K. Hanson, R. Horvath, and M. Geiser, "Dual-comb spectroscopy for high-temperature reaction kinetics," Meas. Sci. Technol. **31**(5), 055501 (2020).
10. D. Burghoff, Y. Yang, D. J. Hayton, J.-R. Gao, J. L. Reno, and Q. Hu, "Evaluating the coherence and time-domain profile of quantum cascade laser frequency combs," Opt. Express **23**(2), 1190 (2015).
11. D. von der Linde, "Characterization of the noise in continuously operating mode-locked lasers," Appl. Phys. B **39**(4), 201–217 (1986).
12. U. Keller, K. Li, M. Rodwell, and D. Bloom, "Noise characterization of femtosecond fiber raman soliton lasers," IEEE J. Quantum Electron. **25**(3), 280–288 (1989).
13. U. Keller, C. E. Soccolich, G. Sucha, M. N. Islam, and M. Wegener, "Noise characterization of femtosecond color-center lasers," Opt. Lett. **15**(17), 974 (1990).
14. J. Hillbrand, D. Auth, M. Piccardo, N. Opačak, E. Gornik, G. Strasser, F. Capasso, S. Breuer, and B. Schwarz, "In-phase and anti-phase synchronization in a laser frequency comb," Phys. Rev. Lett. **124**(2), 023901 (2020).
15. Z. Han, D. Ren, and D. Burghoff, "Sensitivity of SWIFT spectroscopy," Opt. Express **28**(5), 6002 (2020).
16. A. Vardi, G. Bahir, F. Guillot, C. Bougerol, E. Monroy, S. E. Schacham, M. Tchernycheva, and F. H. Julien, "Near infrared quantum cascade detector in GaN/AlGaN/AlN heterostructures," Appl. Phys. Lett. **92**(1), 011112 (2008).
17. D. Hofstetter, M. Beck, and J. Faist, "Quantum-cascade-laser structures as photodetectors," Appl. Phys. Lett. **81**(15), 2683–2685 (2002).
18. H. C. Liu, C. Y. Song, A. J. SpringThorpe, and J. C. Cao, "Terahertz quantum-well photodetector," Appl. Phys. Lett. **84**(20), 4068–4070 (2004).
19. J. Faist, C. Sirtori, F. Capasso, L. Pfeiffer, and K. W. West, "Phonon limited intersubband lifetimes and linewidths in a two-dimensional electron gas," Appl. Phys. Lett. **64**(7), 872–874 (1994).
20. B. F. Levine, "Quantum-well infrared photodetectors," J. Appl. Phys. **74**(8), R1–R81 (1993).
21. H. Liu, J. Li, M. Buchanan, and Z. Wasilewski, "High-frequency quantum-well infrared photodetectors measured by microwave-rectification technique," IEEE J. Quantum Electron. **32**(6), 1024–1028 (1996).
22. P. D. Grant, R. Dudek, M. Buchanan, and H. C. Liu, "Room-temperature heterodyne detection up to 110 GHz with a quantum-well infrared photodetector," IEEE Photonics Technol. Lett. **25**(3), 280–288 (1989).
23. D. Palaferri, Y. Todorov, A. Bigioli, A. Mottaghizadeh, D. Gacemi, A. Calabrese, A. Vasanelli, L. Li, A. G. Davies, E. H. Linfield, F. Kapsalidis, M. Beck, J. Faist, and C. Sirtori, "Room-temperature nine-μm-wavelength photodetectors and GHz-frequency heterodyne receivers," Nature **556**(7699), 85–88 (2018).

24. M. Hakl, Q. Lin, S. Lepillet, J. Lampin, S. Pirotta, R. Colombelli, W. Wan, J. Cao, H. Li, E. Peytavit, and S. Barbieri, "Ultra-fast quantum-well infared photodetectors operating at 10 µm with flat response up to 70ghz at room temperature," arXiv preprint arXiv:2007.00299 (2020).

25. H. Schneider, "Optimized performance of quantum well intersubband infrared detectors: Photovoltaic versus photoconductive operation," J. Appl. Phys. **74**(7), 4789–4791 (1993).

26. A. Harrer, B. Schwarz, S. Schuler, P. Reininger, A. Wirthmüller, H. Detz, D. MacFarland, T. Zederbauer, A. M. Andrews, M. Rothermund, H. Oppermann, W. Schrenk, and G. Strasser, "43 µm quantum cascade detector in pixel configuration," Opt. Express **24**(15), 17041 (2016).

27. B. Schwarz, P. Reininger, A. Harrer, D. MacFarland, H. Detz, A. M. Andrews, W. Schrenk, and G. Strasser, "The limit of quantum cascade detectors: A single period device," Appl. Phys. Lett. **111**(6), 061107 (2017).

28. D. Hofstetter, M. Graf, T. Aellen, J. Faist, L. Hvozdara, and S. Blaser, "23ghz operation of a room temperature photovoltaic quantum cascade detector at 5.35µm," Appl. Phys. Lett. **89**(6), 061119 (2006).

29. T. Dougakiuchi and T. Edamura, "High-speed quantum cascade detector with frequency response of over 20 GHz," in *SPIE Future Sensing Technologies*, C. R. Valenta and M. Kimata, eds. (SPIE, 2019).

30. H. Lotfi, L. Li, L. Lei, H. Ye, S. M. S. Rassel, Y. Jiang, R. Q. Yang, T. D. Mishima, M. B. Santos, J. A. Gupta, and M. B. Johnson, "High-frequency operation of a mid-infrared interband cascade system at room temperature," Appl. Phys. Lett. **108**(20), 201101 (2016).

31. Y. Chen, X. Chai, Z. Xie, Z. Deng, N. Zhang, Y. Zhou, Z. Xu, J. Chen, and B. Chen, "High-speed mid-infrared interband cascade photodetector based on InAs/GaAsSb type-II superlattice," J. Lightwave Technol. **38**(4), 939–945 (2020).

32. B. Schwarz, J. Hillbrand, M. Beiser, A. M. Andrews, G. Strasser, H. Detz, A. Schade, R. Weih, and S. Höfling, "Monolithic frequency comb platform based on interband cascade lasers and detectors," Optica **6**(7), 890 (2019).

33. L. A. Sterczewski, M. Bagheri, C. Frez, C. L. Canedy, I. Vurgaftman, and J. R. Meyer, "Mid-infrared dual-comb spectroscopy with room-temperature bi-functional interband cascade lasers and detectors," Appl. Phys. Lett. **116**(14), 141102 (2020).

34. Z. Xie, J. Huang, X. Chai, Z. Deng, Y. Chen, Q. Lu, Z. Xu, J. Chen, Y. Zhou, and B. Chen, "High-speed mid-wave infrared interband cascade photodetector at room temperature," Opt. Express **28**(24), 36915 (2020).

35. E. Rodriguez, A. Mottaghizadeh, D. Gacemi, D. Palaferri, Z. Asghari, M. Jeannin, A. Vasanelli, A. Bigioli, Y. Todorov, M. Beck, J. Faist, Q. J. Wang, and C. Sirtori, "Room-temperature, wide-band, quantum well infrared photodetector for microwave optical links at 4.9 µm wavelength," ACS Photonics **5**(9), 3689–3694 (2018).

36. S. Ehret, H. Schneider, J. Fleissner, P. Koidl, and G. Böhm, "Ultrafast intersubband photocurrent response in quantum-well infrared photodetectors," Appl. Phys. Lett. **71**(5), 641–643 (1997).

37. S. Steinkogler, H. Schneider, M. Walther, and P. Koidl, "Determination of the electron capture time in quantum-well infrared photodetectors using time-resolved photocurrent measurements," Appl. Phys. Lett. **82**(22), 3925–3927 (2003).

38. H. Schneider and H. C. Liu, *Quantum well infrared photodetectors*, Springer (2007).

39. T. S. Clement, P. D. Hale, K. C. Coakley, and C.-M. Wang, "Time-domain measurement of the frequency response of high-speed photoreceivers to 50 ghz," in *Tech. Dig. Symp. Optical Fiber Measurement* (2000), pp. 121–124.

40. J. Hillbrand, N. Opačak, M. Piccardo, H. Schneider, G. Strasser, F. Capasso, and B. Schwarz, "Mode-locked short pulses from an 8 µm wavelength semiconductor laser," Nat. Commun. **11**(1), 5788–00 (2020).

41. J. Hillbrand, M. Beiser, A. M. Andrews, H. Detz, R. Weih, A. Schade, S. Höfling, G. Strasser, and B. Schwarz, "Picosecond pulses from a mid-infrared interband cascade laser," Optica **6**(10), 1334 (2019).

42. A. S. Kowligy, D. R. Carlson, D. D. Hickstein, H. Timmers, A. J. Lind, P. G. Schunemann, S. B. Papp, and S. A. Diddams, "Mid-infrared frequency combs at 10 GHz," Opt. Lett. **45**(13), 3677 (2020).

43. J. He and Y. Li, "Design of on-chip mid-IR frequency comb with ultra-low power pump in near-IR," Opt. Express **28**(21), 30771 (2020).